Oceanic Variables extracted from Along-Track Interferometric SAR Data

Duk-jin Kim[1] and Wooil M. Moon[1,2]

1. ESI[3] Laboratory, School of Earth & Environmental Sciences Seoul National University, Seoul 151-742, Korea

2. Geophysics, University of Manitoba, Winnipeg, MB R3T 2N2, Canada

(djkim@eos1.snu.ac.kr, wmoon@eos1.snu.ac.kr)

Abstract

The Synthetic Aperture Radar (SAR) data are considered to contain the greatest amount of information among various microwave techniques developed for measuring ocean variables from aircraft or satellites. They have the potential of measuring wavelength, wave direction and wave height of the ocean waves. But, it is difficult to retrieve significant ocean wave heights and surface current from conventional SAR data, since the imaging mechanism of ocean waves by a SAR is determined by the three basic modulation processes arise through the tilt modulation, hydrodynamic modulation and velocity bunching which are poorly known functions. Along-Track Interferometric (ATI) SAR systems can directly detect the Doppler shift associated with each pixel of a SAR image and have been used to estimate wave fields and surface currents. However, the Doppler shift is not simply proportional to the component of the mean surface current. It includes also contributions associated with the phase velocity of the Bragg waves and orbital motions of all ocean waves that are longer than Bragg waves. In this paper, we have developed a new method for extracting the surface current vector using multiple-frequency (L- & C-band) ATI SAR data, and have generated surface wave height information.

Keywords: Along-Track Interferometry, SAR, ocean surface current, wave height

I. Introduction

Synthetic Aperture Radars (SARs) have been used in recent years to image ocean surfaces. They have the potential of measuring wavelength, wave direction, and wave height of the ocean surface waves and current. The mechanisms producing the wave-like modulations in a synthetic aperture radar image have been investigated for many years [Alpers et al.,1981; Hasselmann et al., 1985; Vachon et al., 1994]. The backscattered signal from moving ocean surface is dominated by Bragg scattering from capillary waves and short gravity waves. These waves in turn are modulated in their orientation, energy, and motion by longer waves. But the conventional SAR intensity image over ocean surfaces has some limitations in obtaining quantitative information such as current velocity and wave height, because the radar modulation transfer function (MTF) over the ocean is poorly known and understood.

Recently, airborne Along-Track Interferometric (ATI) SAR has been actively investigated, which has the potential of measuring quantitative information of ocean surface currents and waves [Goldstein and Zebker, 1987; Kim et al., 2002]. The ATI SAR employs two antennas that are separated physically along the platform flight path (along track) direction (Fig. 1).

Until recently, the accurate surface current itself and Bragg wave phase velocities were not extracted from ATI data yet. The ATI SAR systems can directly detect the Doppler shift associated with each pixel of a SAR image. However, the Doppler shift is not simply determined by the mean surface currents. It has various contributions including the phase velocity of the Bragg waves and orbital velocities of all ocean waves and current velocity. In this paper we review some basic ideas of the ATI phase imaging model and describe a method for detecting these contributions. Furthermore, we study the wave field in the off-shore region of Ulsan using ATI images obtained from NASA/JPL AIRSAR.

II. ATI SAR measurements

An Along-Track Interferometric (ATI) SAR is a

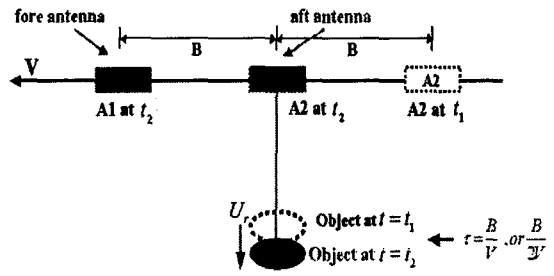

Fig. 1. Principles of Along-Track Interferometric SAR

synthetic aperture radar with two antennas which are separated by some distance along the flight direction (Fig.1). These two antennas image the same area with a short time lag, which cause a phase difference. The phase difference is proportional to the Doppler shift of the backscattered signal and thus to the line-of-sight velocity of the scatterers.

However, Thompson and Jensen [1993] found that a considerable offset between ATI velocities and actual surface currents can occur. Their theoretical explanation for this effect is that the measured ATI phase difference is not determined by the mean surface current but by the mean velocity of the scatterers mapped into a pixel, weighted by the contribution of each scatterer to the backscattered power. The contributions resulting from the velocities of the two Bragg wave components are obtained as well as contributions associated with the orbital motions of longer waves. Their conceptual model in mind is that the pixel-to-pixel phase difference between the two complex SAR images is a measure of the phase of the autocorrelation function $R(\tau)$ of the backscattered field from each pixel at the time lag τ. The complex function $R(\tau)$ is given by

$$R(\tau) = E\{B(t)B^*(t-\tau)\}, \tag{1}$$

where $B(t)$ is the backscattered field from a particular pixel at time t. The autocorrelation function of the backscattered field is related to the Doppler spectrum by

$$R(\tau) = \frac{1}{(2\pi)^{1/2}} \int_{-\infty}^{\infty} e^{i\omega\tau} S(\omega) d\omega \tag{2}$$

where $S(\omega)$ is a real function Doppler spectrum. If the $\omega\tau$ is much smaller than 1, then the phase of autocorrelation function is given by

$$\Delta\phi = \arg\{R(\tau)\} \approx \tau \frac{\int_{-\infty}^{\infty} \omega S(\omega) d\omega}{\int_{-\infty}^{\infty} S(\omega) d\omega} = \bar{\omega}\tau = 2\pi \bar{f}_D \tau \tag{3}$$

where $\bar{f}_D$ is the mean Doppler frequency. This equation states that the pixel-by-pixel phase difference measured by ATI is proportional to the mean Doppler frequency weighted with Doppler spectrum. Romeiser and Thompson [2000] presented an advanced composite surface scattering model that can simulate Doppler spectrum of microwave backscattering from the ocean surface. The key expression of their model can be represented by

$$S(f_D) = \frac{\langle \sigma_+ \rangle}{\sqrt{2\pi\gamma_{D+}^2}} e^{-(f_D - \langle f_{D+} \rangle_\sigma)^2 / \gamma_{D+}^2} + \frac{\langle \sigma_- \rangle}{\sqrt{2\pi\gamma_{D-}^2}} e^{-(f_D - \langle f_{D-} \rangle_\sigma)^2 / \gamma_{D-}^2} \tag{4}$$

$$\langle f_{D\pm} \rangle_\sigma = f_{D\pm}^{(0)} + \mathrm{Re}\left\{ \iint D^*(\mathbf{k}) M_{1\pm}(\mathbf{k}) k^2 \Psi(\mathbf{k}) d^2k \right\}$$

$$\gamma_{D\pm}^2 \equiv \langle f_{D\pm}^2 \rangle_\sigma - \langle f_{D\pm} \rangle_\sigma^2 = \iint D^*(\mathbf{k}) D(\mathbf{k}) k^2 \Psi(\mathbf{k}) d^2k \cdot$$

The $\langle f_{D\pm} \rangle_\sigma$ represents an NRCS-weighted mean Doppler frequency. This will be the center frequencies of the two gaussian Doppler spectrum that corresponds to the backscatter from the two Bragg wave components and that include zeroth-order contributions resulting from the Bragg waves' phase velocity and the mean surface current. The $\gamma_{D\pm}^2$ is the variances determining the Doppler bandwidth or broadness of Doppler spectrum caused by the orbital motions of the long surface waves. Furthermore, D is a linear modulation transfer function (MTF), and Ψ is the spatially varying ocean waveheight spectrum. Then, we may rewrite equation (3) as

$$\begin{aligned} \Delta\phi = \arg\{R(\tau)\} &= \frac{2\pi\tau}{\langle\sigma\rangle} \int_{-\infty}^{\infty} f_D S(f_D) df_D \\ &= 2\pi\tau \left\{ A \int_{-\infty}^{\infty} f_D S_+(f_D) df_D + B \int_{-\infty}^{\infty} f_D S_-(f_D) df_D \right\} \\ &= 2\pi\tau \left\{ A \langle f_{D+} \rangle_\sigma + B \langle f_{D-} \rangle_\sigma \right\} \end{aligned} \tag{5}$$

where the Doppler spectrum is normalized and the Doppler spectrum is separated into two Bragg wave components using weighting factor A and B. The weighting factor A and B include NRCS mean values

corresponding to each Bragg wave component. Because the mean value of the gaussian distribution is the center frequency of each Bragg wave contributions, the phase difference can be expressed by the sum of weighted mean Doppler frequencies of each Bragg wave components. Fig. 2 show that the mean Doppler frequency of Doppler spectrum is not equal to the Bragg resonant frequency, but they can have the same mean Doppler frequency value regardless of Doppler bandwidth when the ratio of weighting factor is same.

In this study, we decomposed NRCS-weighted mean Doppler frequencies into four contributions as

$$\langle f_{D\pm} \rangle_a = f_D^c + f_{D\pm}^b + f_{D\pm}^m + f_D^o \tag{6}$$

where f_D^c is the contributions of the mean surface current, f_C^o is the contributions of the phase velocities of the two Bragg wave components, $f_{D\pm}^m$ is the contributions of the correlated NRCS variations, and $f_{D\pm}^b$ is the contributions of the orbital velocities of the long gravity waves which change periodically.

III. Ocean surface current and wave estimations

The ATI SAR measures the NRCS-weighted mean Doppler frequency, which is a sum of four contributions (Eq. 6). To estimate surface current component, we have to remove the last three terms. The fourth term ($f_{D\pm}^b$) can be removed by spatial averaging over large areas due to their periodicity. In addition, the correlated NRCS variations ($f_{D\pm}^m$) that are related to the modulation transfer function depend on sea states. If the sea surface wind is low, this contribution may be very small at the moderate incidence angles during averaging process, and one can neglect this contributions. Under these conditions, we can express Eq. 5 as

$$\begin{aligned} \langle \Delta\phi \rangle_s &= \langle \arg\{R(\tau)\} \rangle = 2\pi\tau \{ A\langle f_{D+} \rangle_a + B\langle f_{D-} \rangle_a \} \\ &= 2\pi\tau \{ A(f_D^c + f_{D+}^b) + B(f_D^c + f_{D-}^b) \} \\ &= 2\pi\tau \{ f_D^c + Af_{D+}^b + (1-A)f_{D-}^b \} \\ &= 2\pi\tau \{ f_D^c + (2A-1)f_{D+}^b \} \cdot \end{aligned} \tag{7}$$

This equation states that the spatially averaged phase difference of the ATI in the low wind sea states is the sum of current contribution frequency and the Bragg waves related term. The current frequency does not depend on the mean NRCS, but it shifts the entire Doppler spectrum. Therefore the current frequency can factor out. To satisfy this condition, the weighting factor B should be 1-A. Finally, one can obtain the resulting equation represented in terms of frequency using ATI parameters.

$$\langle U \rangle_s = \frac{\lambda}{4\pi\tau} \langle \Delta\phi \rangle_s = \frac{\lambda}{2} \{ f_D^c + (2A-1)f_D^b \} = v_c + (2A-1)c_p \tag{8}$$

The v_c is a surface current velocity, and c_p is a resonant Bragg wave phase velocity when antennas look directly upwind.

From the Eq. 8, we tried to develop a new method for extracting the ocean surface current. The effectively averaged velocities of the L-band and C-band ATI data are the sum of surface current and Bragg wave related components. The Bragg wave related components will be the net Bragg wave phase velocity that is affected by the ratio of the spectral densities of advancing and receding waves within the resolution cell, that is α and 1-α, respectively,

$$\langle U \rangle_s^L = v_c^L + [2\alpha^L(\theta_w) - 1]c_p^L \quad \langle U \rangle_s^C = v_c^C + [2\alpha^C(\theta_w) - 1]c_p^C \tag{9}$$

In this equation, we can suppose that the ocean surface current is steady over relatively wide area regardless of

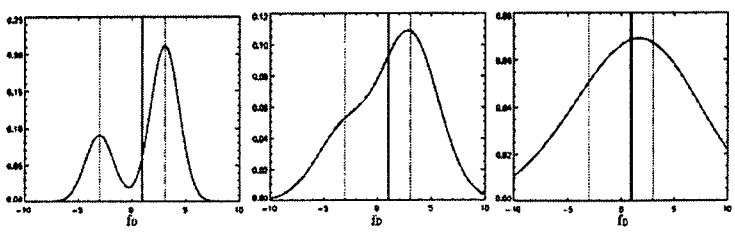

Fig. 2. Simulated normalized Doppler spectra obtained from Romeiser and Thompson [2000] model.

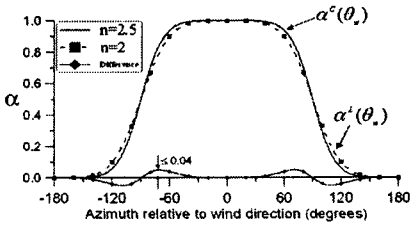

Fig. 3. Respective proportions of approaching Bragg-resonant wave spectral density contributing to the radar echo

radar frequency, while the net Bragg wave phase velocities depend on radar frequency. Therefore, the difference between L- and C-band's spatially averaged velocity is caused by the net Bragg wave phase velocity difference. Since Kim et al. [2002] were proved that the α^L and α^C values which depend on wind direction are equal (Fig. 3), the difference between L-band and C-band averaged velocities can be expressed as

$$\begin{aligned}\langle U\rangle^L - \langle U\rangle^C &= [2\alpha^L(\theta_\downarrow)-1]c_r^L - [2\alpha^C(\theta_\downarrow)-1]c_r^C \\ &= [2\alpha(\theta_\downarrow)-1](c_r^L - c_r^C)\end{aligned} \quad (10)$$

This equation states that the α value and the wind direction information can be extracted from the difference between the multiple frequencies ATI SAR data. Furthermore, one can extract the Bragg wave phase velocities and the ocean surface current ($\langle U\rangle - [2\alpha - 1]c_r$) at each frequency ATI SAR data.

The conventional SARs have the potential of measuring ocean surface wave information. The three basic modulation processes are the tilt modulation caused by local incidence angle variation of the facet through the long wave slope, the hydrodynamic interaction between short and long waves, and motion effects (velocity bunching), which produce a Doppler shift in the return signal and induce an azimuthal displacement of the scattering element in the SAR image. An important feature of the process is that SAR imaging is typically nonlinear. Although the hydrodynamic and tilt modulation can usually be approximated as linear processes, the velocity bunching mechanism associated with the orbital motion of the long waves is strongly nonlinear.

However, the ATI SAR can detect directly the line-of-sight velocity, which has four contributions (Eq. 6). The phase velocity of Bragg wave and the ocean surface current velocity are usually steady over large areas, whereas the periodical orbital velocity due to swell is composed higher spatial variability. These allow us to obtain the wavelength and propagation direction of dominant ocean waves. The wave period and velocity are calculated from the linear dispersion relation

$$\omega = \frac{2\pi}{T} = \sqrt{kg\ \tanh(kh)} \quad (11)$$

where, g is the acceleration due to gravity, k is the wavenumber of the swell, and h is the water depth. The line-of-sight velocity component can be appropriately transformed to real orbital velocity component of waves using the factor [Alpers and Rufenach, 1979]

$$\frac{1}{G} = 1\Big/\sqrt{\sin^2\phi + \cos^2\theta\cos^2\phi}\ . \quad (12)$$

This factor is purely geometric and depends on the incidence angle (θ) and the angle between the wave propagation direction and the aircraft flight direction (ϕ) The angular velocity of each orbiting scattering element is related to the wavelength and the water depth through the linear dispersion relationship. Therefore, the wave height can be extracted simply by dividing the twice orbital velocity with the angular velocity as

$$H = 2\hat{U}_r\Big/G\omega \quad (13)$$

where, the $\hat{U}_r$ is amplitude of the radial velocity.

IV. Experimental results

We have processed ATI data from PACRIM-II mission on September 30th, 2000 over the Ulsan coast off the southeast shore of the Korean peninsula. During the PACRIM-II Korea mission, two lines of ATI data were collected and the two ATI lines are approximately at right angle to each other (Fig. 4). Currently, a part of the 197 line ATI data was used to investigate the ocean surface current. The time difference between the two orthogonal data acquisition flights is approximately 18 minutes, and the wind was calm during this period.

To extract exact velocity from ATI data, phase calibration processing should be correctly carried out first. The flat earth phase that was caused by a cross-track baseline component and additional phase bias were removed by subtracting the non-zero phase difference over the land at the sea level. And the calibrated phase difference was converted to the line-of-sight velocity using the AIRSAR parameters. All ATI images used in

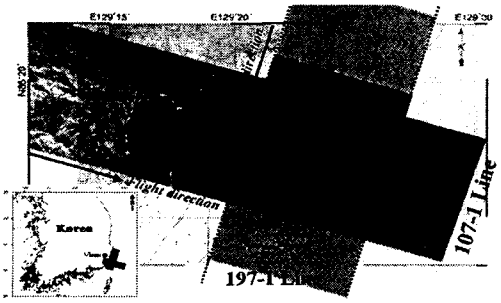

Fig. 4. Study area. The image is the magnitude image of LAA test data and topography as base map.

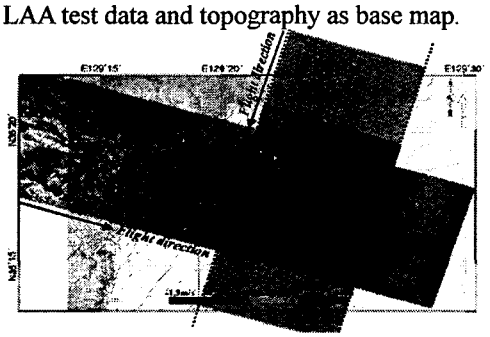

Fig. 5. Calibrated resulting interferometry velocity map calculated from ATI equation.

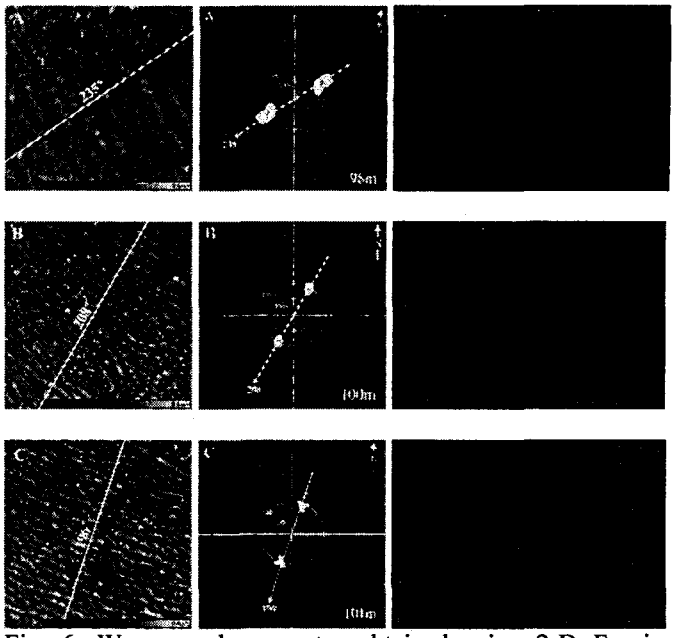

Fig. 6. Wave number spectra obtained using 2-D Fourier transform of the interferometry velocity map (Fig. 5) and wave height at the sub area A, B, and C.

Table I. Test Results estimated from the two-dimensional wave number spectra and linear dispersion relation corresponding to sub area A, B and C.

	A	B	C
Image Size	1024m×1024m	2048m×2048m	2048m×2048m
Incidence Angle	27.0°	38.7°	38.8°
Mean Depth	-38m	-65m	-92m
Wavelength	98m	100m	101m
Wave Direction	235°	208°	196°
Wave Period	7.99s	8.01s	8.05s
Wave Velocity	12.3m/s	12.5m/s	12.5m/s

this study were converted to ground range images which have equal pixel spacing, and the L- and C-band ATI data were properly registered to extract current components. This registration step was carried out using a re-gridding scheme (SCH-coordinate).

The calibrated radial velocity maps were generated for 197 path and 107 path data using ATI equation, respectively (Fig. 5). In the 107 path velocity map, we can see that the negative velocity over the ocean, which correspond to water scatters' propagating toward the aircraft that is, downward in this figure. In this figure, we can also observe the wave-like patterns that propagate obliquely with respect to the coastal line and refraction and shoaling as it approaches the shore.

For the periodicity of the orbital velocity of swell, we can facilitate Fourier analysis. Fig. 6 are the wavenumber spectra obtained using 2-D Fourier transform of the velocity map from the sub area A, B and C in Fig. 5, respectively. The dominant wavelength of all sub areas shows similar results, but the propagation direction varies at each sub area. The resulting swell systems of sub-area A, B and C are summarized in Table I. The ocean surface wave velocity and height images estimated using Eq. 13 at each sub area are also shown in Fig. 6.

To estimate the sea surface current velocity using the equations discussed in section III, the line-of-sight component velocity was converted to horizontal velocity. Then spatial moving averaging was carried out to remove spatially varying components such as swell and orbital motions of long ocean waves. But this processing may not always be effective or correct way of removing orbital motion effects, where strong current gradients or internal waves were present. Since these effects can modulate the backscattered signal both in amplitude and frequency, one should also reconsider the above approach when there is strong wind blowing. Despite of these limitations, the current field extraction proposed in this study is valid and can be practically useful. Fig. 7 shows

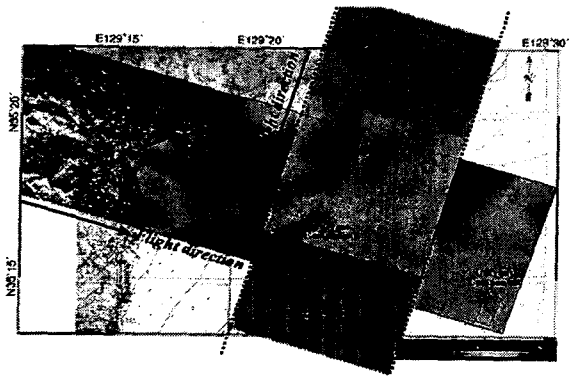

Fig. 7. The resulting current velocity (vector) image extracted from multiple (L- & C-band) ATI data.

the resulting surface current velocity using the equations (Eq. 9 and Eq. 10) derived in this study. With the assumption that the large scale surface current field does not change too much during the 18min period, we estimated the surface current vector in the common region (Fig. 7). A high surface current velocity in the left side region may be caused by the low coherence resulting from a short decorrelation time.

V. Summary and conclusion

We used ATI SAR data that were collected during the PACRIM-II AIRSAR campaign over the Ulsan coast off the southeast shore of the Korean peninsula to investigate the ocean waves and current features. In this study, we have reviewed how the phase difference measured by ATI is related to the mean Doppler frequency, and developed a new method to extract surface current component from L- & C-band ATI data, and have extracted ocean surface current vectors over the off-shore Ulsan area. On the other hand, we were able to retrieve the wavelength, direction, period, velocity, and wave height of the ocean surface waves using the linear dispersion relationship and Fourier analysis techniques from the ATI SAR data.

Acknowledgment

This study is partially funded by the BK21 program through School of Earth and Environmental Sciences (SEES), Seoul National University and partially by NSERC operating grant (A-7400) to Wooil M. Moon.

References

W. Alpers and C. Rufenach, 1979, The effect of orbital motions on synthetic aperture radar imagery of ocean waves, IEEE Trans. Antennas Propag., AP-27(5), 685-690.

W.R. Alpers, D.B. Ross, C.L. Rufenach, 1981, On the detectability of ocean surface waves by real and synthetic aperture radar, J. Geophys. Res., Vol. 86, No. C7, 6481-6498.

R.M. Goldstein and H.A. Zebker, 1987, Interferometric radar measurement of ocean surface currents, Nature, Vol. 328, 707-709.

K. Hasselmann, R.K. Raney, W.J. Plant, W. Alpers, R.A. Shuchmanm, D.R. Lyzenga, C.L. Rufenach and M.J. Tucker, 1985, Theory of synthetic aperture radar ocean imaging; A MARSEN view, J. Geophys. Res., Vol. 90, 4659-4686.

D.-j Kim, W.M. Moon, D.A. Imel and D. Moller, 2002, Investigation of ocean waves and currents using NASA (JPL) AIRSAR Along-Track Interferometry (ATI), IEEE Trans. Geoscience and Remote sensing, submitted.

R. Romeiser and D.R. Thompson, 2000, Numerical study on the Along-Track Interferometric radar imaging mechanism of oceanic surface currents, IEEE Trans. Geoscience and Remote sensing, Vol. 38, No. 1, 446-458.

D.R. Thompson and J.R. Jensen, 1993, Synthetic aperture radar Interferometry applied to ship-generated internal waves in the 1989 Loch Linnhe experiment, J. Geophys. Res., Vol. 98, No. C6, 10259-10269.

P.W. Vachon, H.E. Krogstad, J.S. Paterson, 1994, Airborne and spaceborne synthetic aperture radar observations of ocean waves, Atmosphere-Ocean, Vol. 32(1), 83-112.